AN INVESTIGATION OF THE MATERIAL PROPERTIES OF LASER SINTERED PARTS INCORPORATING CONFORMAL LATTICE STRUCTURE (CLS™) TECHNOLOGY

A. L. Cooke[1], C. E. Folgar[1], L. N. Folgar[1], J. Williams[1], S. Park[2], D. W. Rosen[2]

[1]3D Systems Corporation, Rock Hill, SC 29730
[2]School of Mechanical Engineering, Georgia Institute of Technology, Atlanta, GA 30332

Abstract

Cellular materials, including foams, honeycombs, lattices, and similar constructions, offer the key advantages of high strength-to-weight ratios and favorable energy absorption characteristics. The concept of designed cellular materials enables customized material placement to best suit the demands of specific applications or achieve particular performance targets. The design, generation, and fabrication of conformal lattice structures via laser sintering are at the center of the disruptive manufacturing technologies proposed by 3D Systems Corporation. The primary work reported here is the maturation and mechanical testing of the conformal lattice structure technology developed between 3D Systems Corporation and the Georgia Institute of Technology.

Introduction

Selective laser sintering (SLS[1]) is a form of additive manufacturing (AM), a layer-wise fabrication technique that is increasingly being used to manufacture functional parts. The commercially available materials used in the ploymer-based processes have been limited to nylons. Direct part manufacturing of aerospace components is an application that requires the use of engineered polymers with superior mechanical performance, intelligently engineered structures, and advanced process controls with a combination of post processing techniques that can enhance the ultimate performance of a given part.

Designed Cellular Materials

Figure 1 displays examples of cellular materials, which include foams, honeycombs, lattices, and similar constructions. From a mechanical engineering viewpoint, a key advantage offered by cellular materials is high strength accompanied by a relatively low mass. These materials can also present good energy absorption characteristics (e.g. acoustic attenuation and vibration damping), and when incorporated into designs for thermal applications they can provide good thermal insulation [1]. The work presented here focuses on lattice structures.

Throughout the past two decades research pertaining to lattice materials has proliferated due to their advantage of providing lighter, stronger, and stiffer materials than foams [2]. More recently, conformal lattice structure (CLS[2]) technology has been introduced and detailed in

[1] SLS® is a registered trademark of 3D Systems Corporation.
[2] CLS™ is a trademark of 3D Systems Corporation.

various venues [3-5]. Figure 2 displays a graphic illustrating the difference between a uniform lattice structure and a conformal lattice structure.

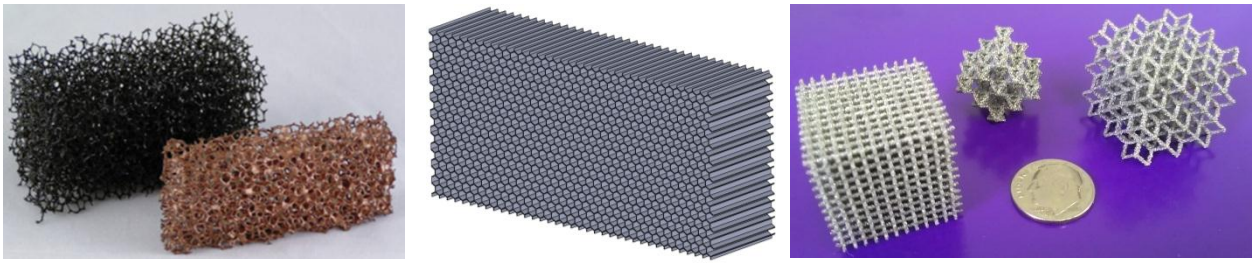

(a) (b) (c)

Figure 1: Examples of cellular materials: (a) foam [6], (b) honeycomb, and (c) lattice

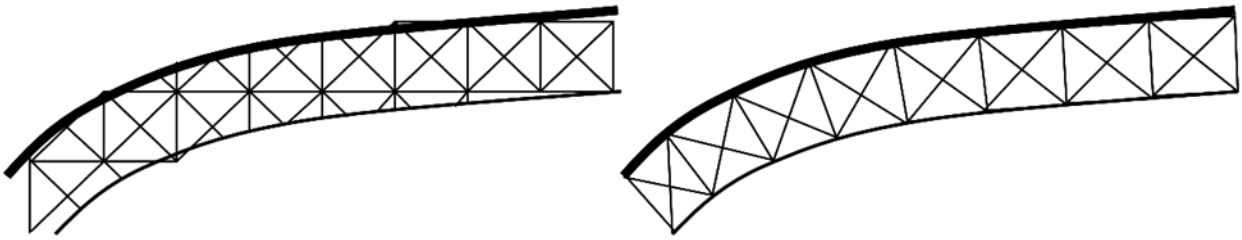

(a) (b)

Figure 2: Visual comparison between lattice structures: (a) uniform and (b) conformal

The concept of designed cellular materials is motivated by the desire to put material only where it is needed for a specific application or for a specific target performance. As evidenced by the image in Figure 2(b), the lattice structure in the conformal configuration corresponds to the geometry's surface and aligns to the load plane producing predictable testing and performance behavior. 3D Systems Corporation and Georgia Institute of Technology have jointly developed a technology that automates the creation of CLSes[3] [7]. The schematic in Figure 3 provides a flowchart depicting the creation and optimization of CLSes applied to solid models. After a part is designed in a computer-aided design (CAD) software a plugin called TrussCreator is then used to create lattice structure on selected surfaces or volumetric regions based on specified lattice structure parameters, including unit cell size and type, orientation of lattice structure, and tolerances on merging nodes and edges if they are close.

The creation of the initial lattice structures in the TrussCreator plugin serves as the first step in an iterative process. For step two, the initial lattice is imported into a simulation package where boundary conditions are configured and loads are applied in order to determine the selected parameters' adequacy. If the lattice structures fail in the simulations, then the two steps are repeated until the resulting geometry is satisfactory. Then the final geometry returns to the CAD software where it can be saved as a solid part file.

[3] CLSes is used throughout this document as the plural form of CLS.

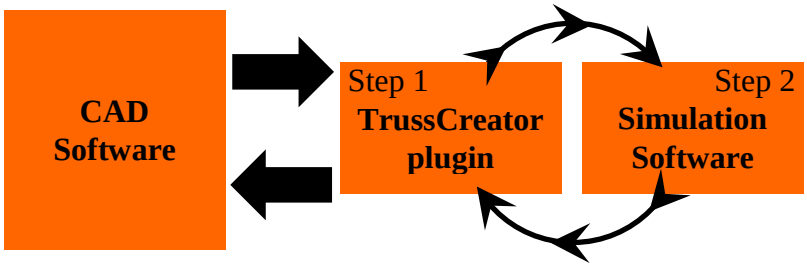

Figure 3: Process of creating and optimizing CLSes

Mechanical Properties Testing

When analyzing the behavior of the latticed geometry in the second step of the iterative process depicted in Figure 3, a very important assumption is made. That assumption is that the material properties are independent of the final part's build orientation. The goal of the work presented here was to investigate the resulting properties of CLSes. To do this, sets of Nylon 12 test specimens were built and underwent a battery of ASTM testing. We wanted to evaluate the properties of the individual struts making up the lattice structures as well as the properties of the lattice structures formed by the individual struts.

Individual Struts

In order to evaluate the individual struts, structures (hereafter referred to as "peacocks") were designed to enable single struts to be built in specific orientations. Illustration of a single strut and its arrangement with others to form the "peacock" are provided in Figure 4. The struts were designed to be used as-built for tensile testing or simply altered to create the other geometries necessary for different test methods. As built, the struts were connected to a sphere by a rod less than 1 mm in diameter to enable easy removal. A total of 23 struts comprised each "peacock" structure. Figure 5 illustrates the strut locations and the labeling schema that was followed. A total of 60 "peacocks" were produced with struts of 1 mm, 2 mm, and 5 mm, for a total of 1,380 struts. To reduce the expense of testing all 1,380 struts, 780 struts (13 per "peacock") were selected for testing at an outside facility. The battery of testing included those for evaluating tensile, compressive, and flexural properties in accordance with applicable ASTM standards. The struts tested are shown in Figure 5, and they are tabulated in Table 1.

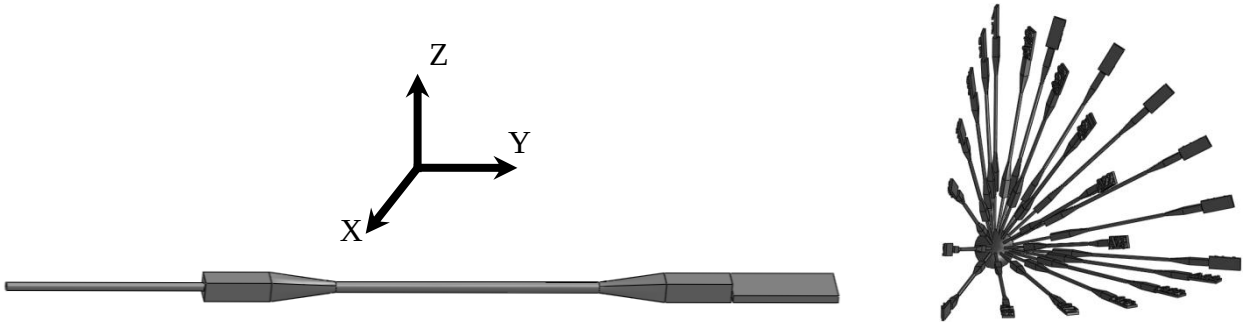

Figure 4: Illustrations of (a) an individual strut and (b) the "peacock" structure.

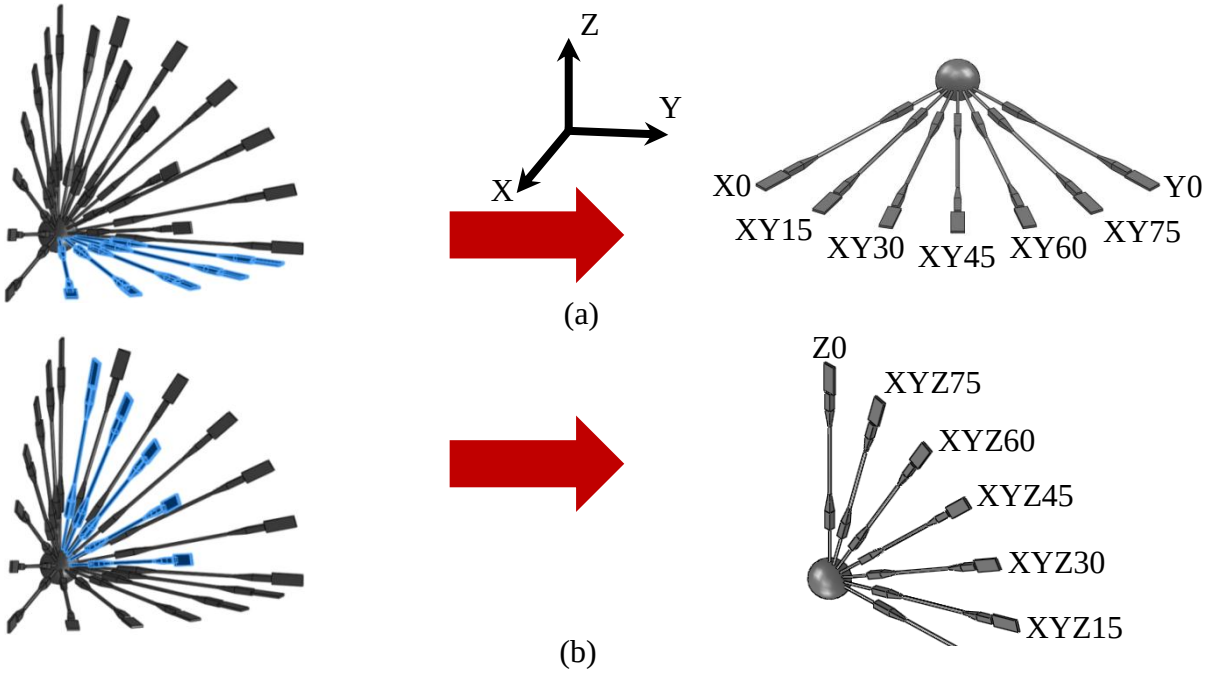

Figure 5: Illustrations depicting the locations of the 13 tested struts and their labelling schema; (a) XY plane and (b) XYZ plane.

Table 1: The 13 "peacock" struts tested at an outside facility.

Label	Build Orientation
X0	Parallel with the X axis of the machine
Y0	Parallel with the Y axis of the machine
Z0	Parallel with the Z axis of the machine
XY15	Parallel with the XY plane and offset 15° from the X axis of the machine
XY30	Parallel with the XY plane and offset 30° from the X axis of the machine
XY45	Parallel with the XY plane and offset 45° from the X axis of the machine
XY60	Parallel with the XY plane and offset 60° from the X axis of the machine
XY75	Parallel with the XY plane and offset 75° from the X axis of the machine
XYZ15	Parallel with a plane bisecting the 90° angle formed by the YZ and XZ planes and offset 15° from the XY plane
XYZ30	Parallel with a plane bisecting the 90° angle formed by the YZ and XZ planes and offset 30° from the XY plane
XYZ45	Parallel with a plane bisecting the 90° angle formed by the YZ and XZ planes and offset 45° from the XY plane
XYZ60	Parallel with a plane bisecting the 90° angle formed by the YZ and XZ planes and offset 60° from the XY plane
XYZ75	Parallel with a plane bisecting the 90° angle formed by the YZ and XZ planes and offset 75° from the XY plane

In ASTM D638 [8], tensile properties are determined by subjecting test specimens to an increasing uniaxial tension, shown schematically in Figure 6. The geometry requirement for the test specimens dictated no change in the as-built struts. Table 2 displays the yield strength values determined from the tensile tests for each strut diameter. Figure 8 immediately follows and displays plots of the values with respect to build orientations and strut diameters. Each data point is the mean value of results from five tests, and the error bars represent one standard deviation.

Figure 6: Tensile test schematic (shown horizontally).

Table 2: ASTM D638 tensile testing results for the 1 mm, 2 mm, and 5 mm struts.

Label	Strength at Yield		
	1 mm Struts	2 mm Struts	5 mm Struts
	MPa	MPa	MPa
X0	23.4	31.6	52.5
Y0	24.2	31.1	46.2
Z0	30.4	43.1	44.5
XY15	26.1	30.4	46.4
XY30	26.5	30.7	45.9
XY45	29.4	31.4	45.6
XY60	26.9	34.4	45.7
XY75	25.9	34.7	45.7
XYZ15	29.5	33.1	44.6
XYZ30	30.3	32.6	44.4
XYZ45	30.6	32.3	45.0
XYZ60	31.3	32.8	44.8
XYZ75	31.8	41.1	44.6

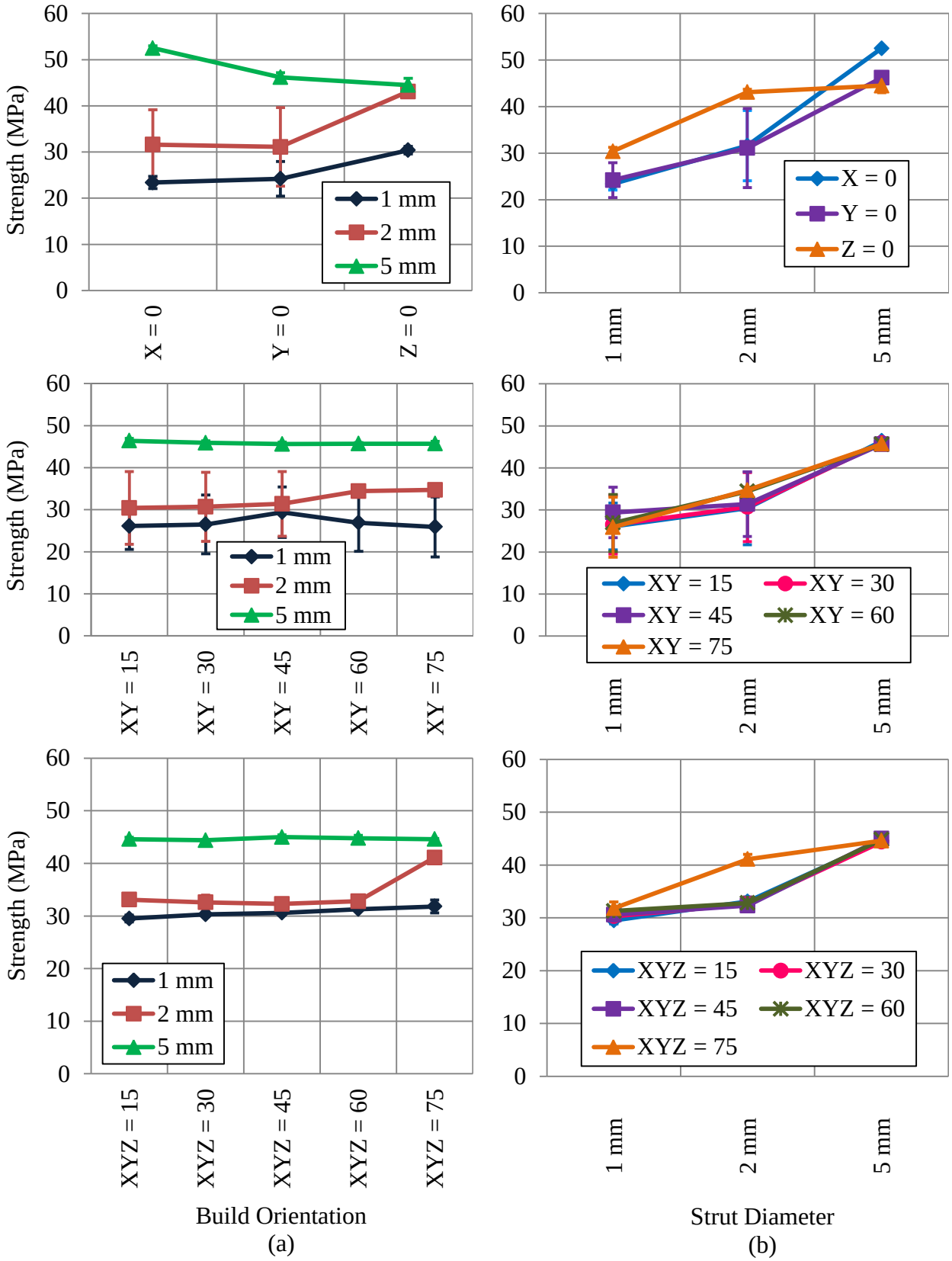

Figure 7: Tensile strength at yield vs. (a) build orientation and (b) strut diameter.

In ASTM D695 [9], compressive properties are determined by subjecting a specimen placed on a hardened surface to an increasing compressive force caused by lowering a plunger onto it. This is shown schematically in Figure 8. The geometry requirement for the test specimens required the removal of right cylinders from the gage length of each strut. Table 3 displays the values of compressive strength at yield determined from the compressive tests. Figure 9 immediately follows Table 3 and displays separate plots of the tabulated values with respect to build orientations and strut diameters. Data points are mean values of results from five runs, and error bars are one standard deviation.

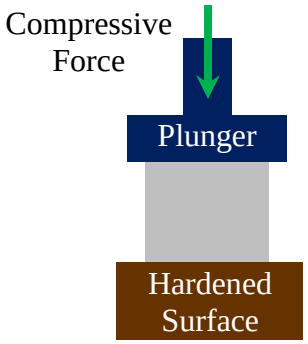

Figure 8: Compression test schematic.

Table 3: ASTM D695 compression testing results for the 1 mm, 2 mm, and 5 mm struts.

Label	Strength at Yield		
	1 mm Struts	2 mm Struts	5 mm Struts
	MPa	MPa	MPa
X0	41.7	31.4	52.9
Y0	32.6	30.9	46.5
Z0	39.2	47.4	45.7
XY15	31.4	25.8	40.3
XY30	39.8	24.3	44.0
XY45	34.4	23.6	42.8
XY60	35.3	30.3	40.8
XY75	33.5	26.6	48.3
XYZ15	32.2	28.9	41.6
XYZ30	32.8	34.2	43.5
XYZ45	34.4	32.4	40.9
XYZ60	37.7	37.9	43.1
XYZ75	45.0	39.9	45.0

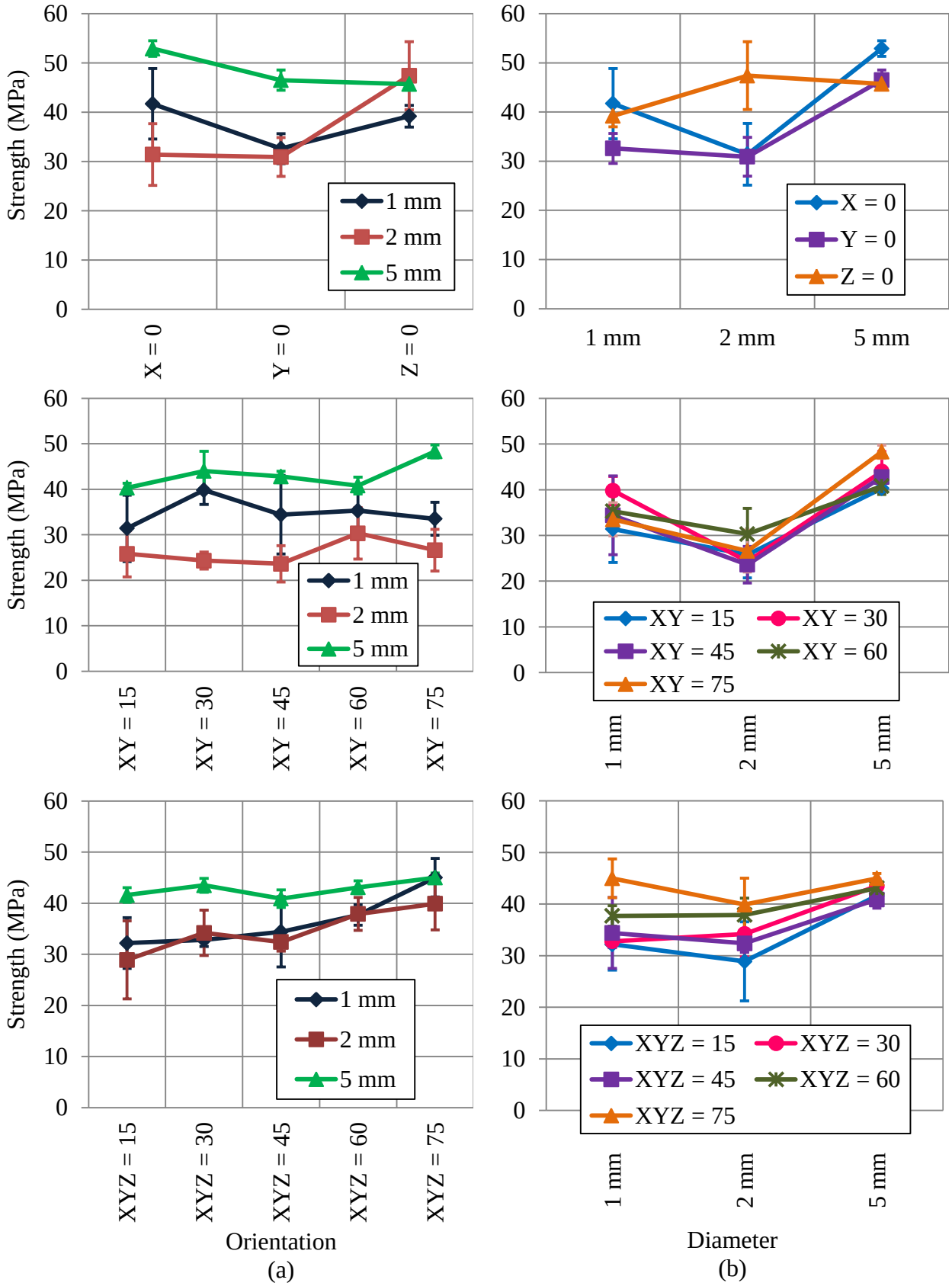

Figure 9: Compression strength at yield vs. (a) build orientation and (b) strut diameter.

In ASTM D790 [10], flexural properties are determined utilizing a three-point loading system applied to a simply supported beam, a rectangular prism cut from the center of the "peacock's" struts. This is shown schematically in Figure 10. Table 4 displays the flexural strength values determined from the flexural tests. Figure 11 displays plots of flexural strength with respect to build orientations and strut diameters. Each data point is the mean value of results from five tests, and the error bars represent one standard deviation.

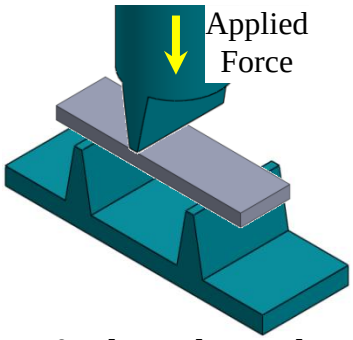

Figure 10: Flexural test schematic.

Table 4: ASTM D790 flexural testing results for the 1 mm, 2 mm, and 5 mm struts.

Label	Strength		
	1 mm Struts	2 mm Struts	5 mm Struts
	MPa	MPa	MPa
X0	49.9	41.6	65.4
Y0	25.9	47.9	77.4
Z0	40.7	78.4	61.2
XY15	41.4	52.2	76.8
XY30	35.1	51.7	80.6
XY45	37.4	51.3	86.0
XY60	35.4	51.1	89.3
XY75	35.1	48.0	91.2
XYZ15	40.4	43.8	73.5
XYZ30	42.5	55.0	77.0
XYZ45	43.3	49.8	69.6
XYZ60	43.6	53.4	71.4
XYZ75	77.8	74.2	73.4

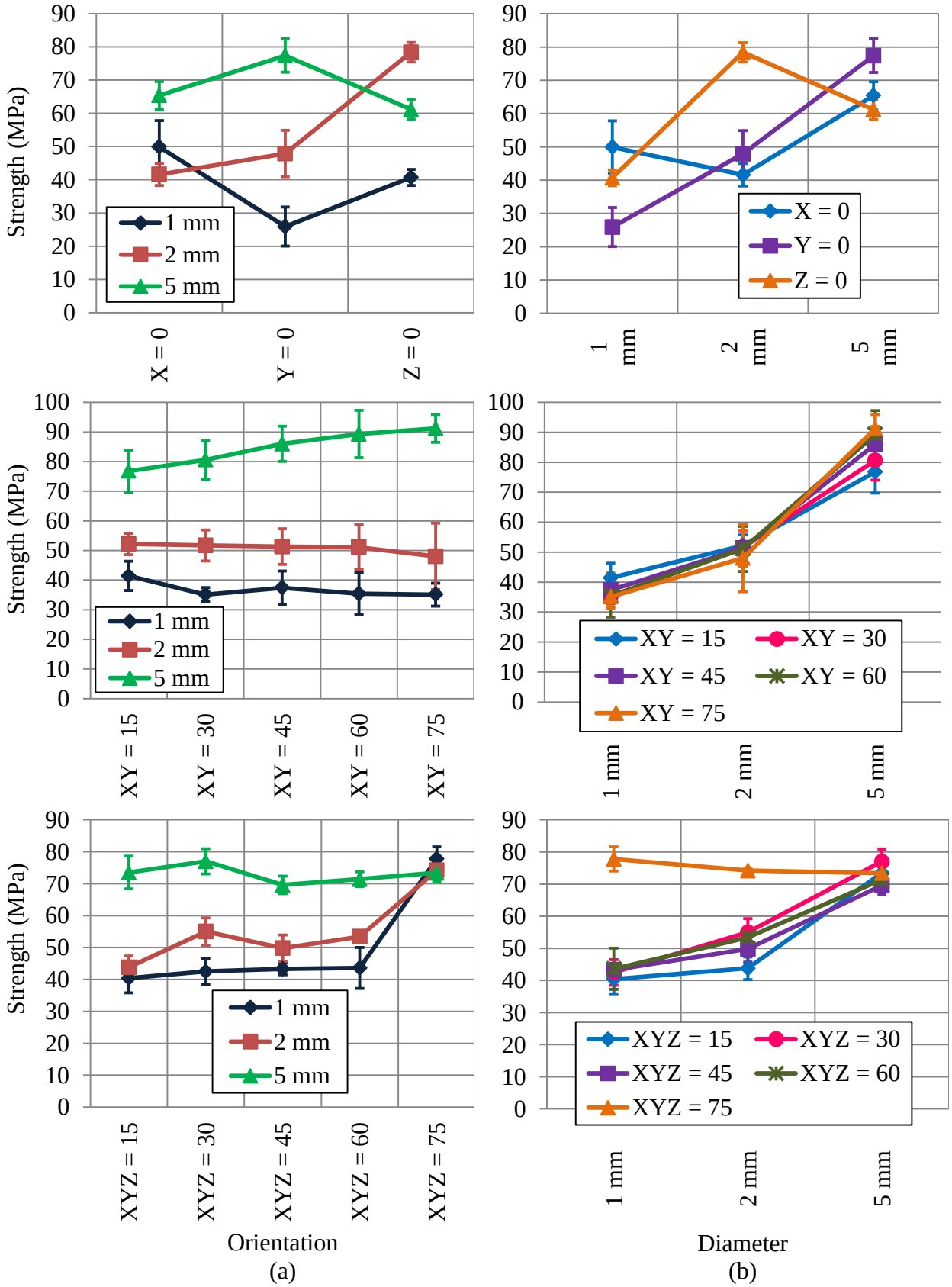

Figure 11: Flexural strength vs. (a) build orientation and (b) strut diameter.

Conformal Lattice Structures

After all testing on the "peacock" struts was completed, the next step was to perform a battery of tests on actual CLSes. An illustration of a CLS is provided in Figure 12.

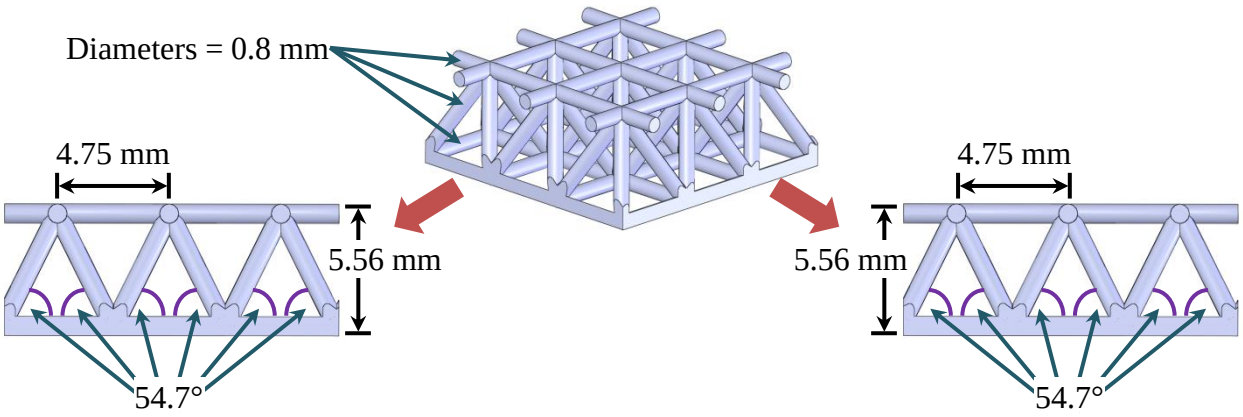

Figure 12: Illustration of a conformal lattice structure (CLS).

The CLS displayed in Figure 12 is one layer thick. A layer consists of three sections: a top and bottom array of orthogonal bars (Fig. 13(a) and 13(b)), and an adjoining section comprised of orthogonal rows of connective trusses (Figs. 13(d) and 13(e)). The top section is centered above the bottom section as shown in Figure 13(c), and the middle section of trusses is inserted between them to form the geometry shown in Figure 12. As layers are added, the top and bottom sections are shared. Figure 14 displays nine different types of CLSes built and tested for tensile, compressive, and shear properties in accordance with applicable ASTM standards. The freedom of AM allowed each test specimen to be built to the required dimensional specifications. The labeling scheme in Figure 14 is further explained in Table 5.

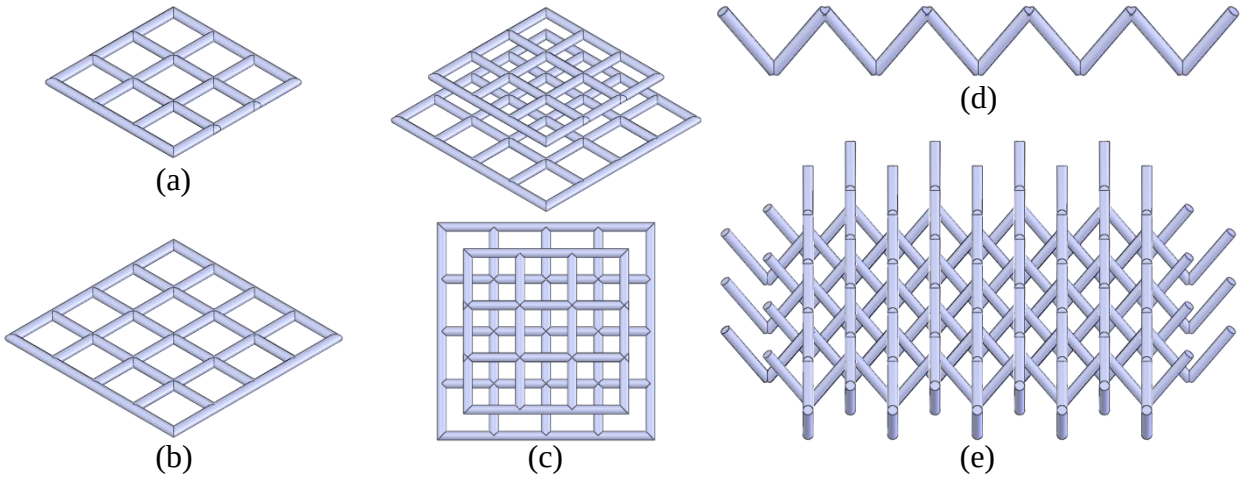

Figure 13: CLS construction: (a) top section, (b) bottom section, (c) top and bottom section alignment, (d) single row of connective trusses, and (e) orthogonal arrangement of connective truss rows.

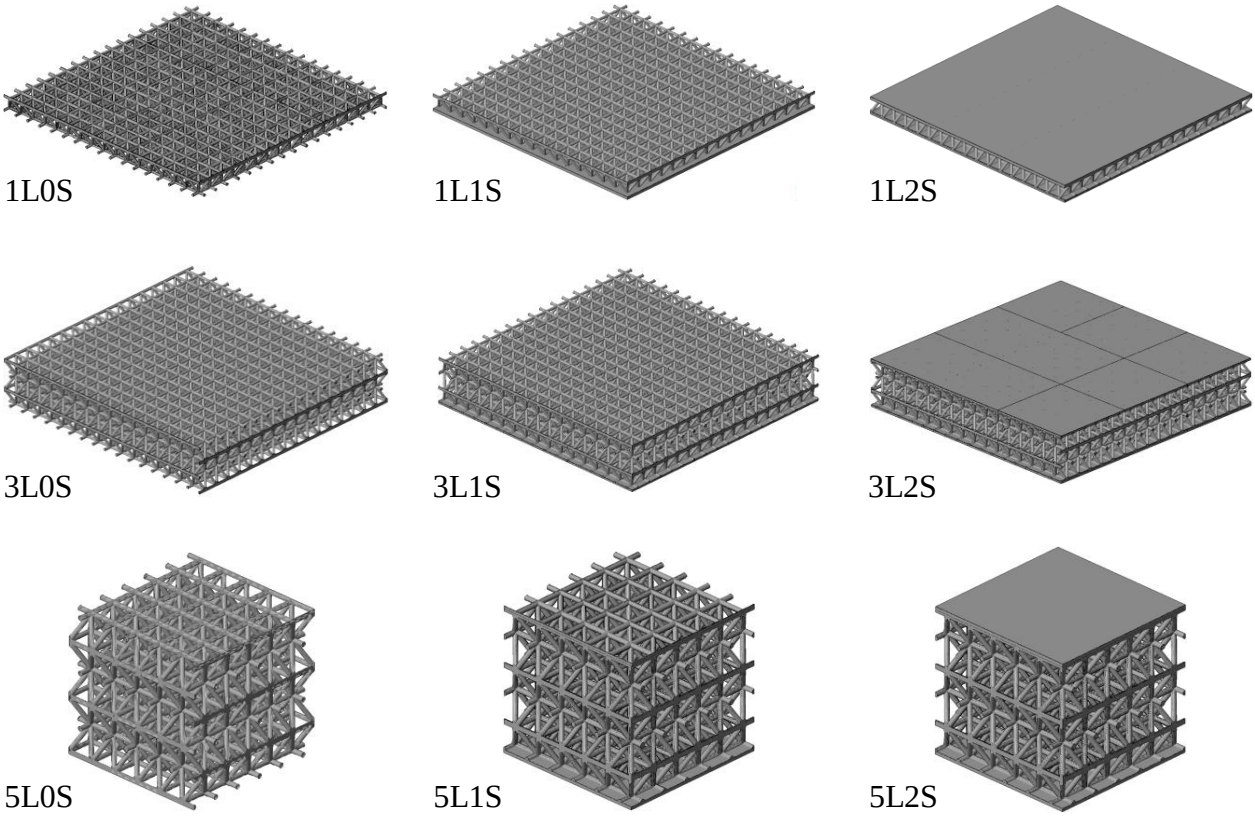

Figure 14: Nine CLS types built and tested for tensile, compressive, and shear properties.

Table 5: Descriptions of the nine types of CLSes tested.

Label	Description
1L0S	one layer and no skins*
1L1S	one layer and one skin
1L2S	one layer and two skins
3L0S	three layers and no skins
3L1S	three layers and one skin
3L2S	three layers and two skins
5L0S	five layers and no skins
5L1S	five layers and one skin
5L2S	five layers and two skins

*A skin is a solid sheet of material that covers the top and/or bottom of a CLS.

In ASTM C297 [11], tensile properties of the CLS are determined by subjecting test specimens to an increasing uniaxial tension. As shown schematically in Figure 15, loading blocks were bonded to the skins of the CLS or directly to the core if there was no skin. Table 6 displays the ultimate flatwise tensile strength values determined from the tests. Figure 16 shows the behavior of the properties with respect to number of layers and number of skins. Each data point is the mean value of results from five tests, and the error bars represent one standard deviation.

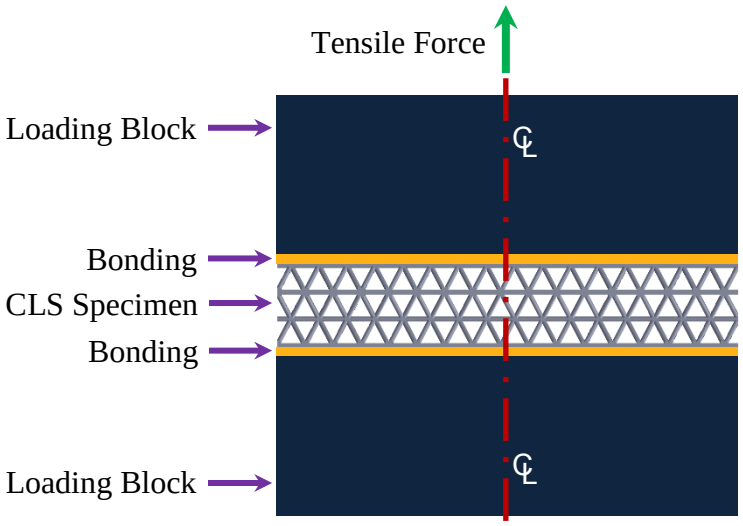

Figure 15: Schematic of specimen arrangement during ASTM C297 testing.

Table 6: ASTM C297 testing results for the nine CLS types tested.

Label	Ultimate Flatwise Tensile Strength MPa
1L0S	1.29
1L1S	1.24
1L2S	1.05
3L0S	1.03
3L1S	0.74
3L2S	1.07
5L0S	1.57
5L1S	1.34
5L2S	1.37

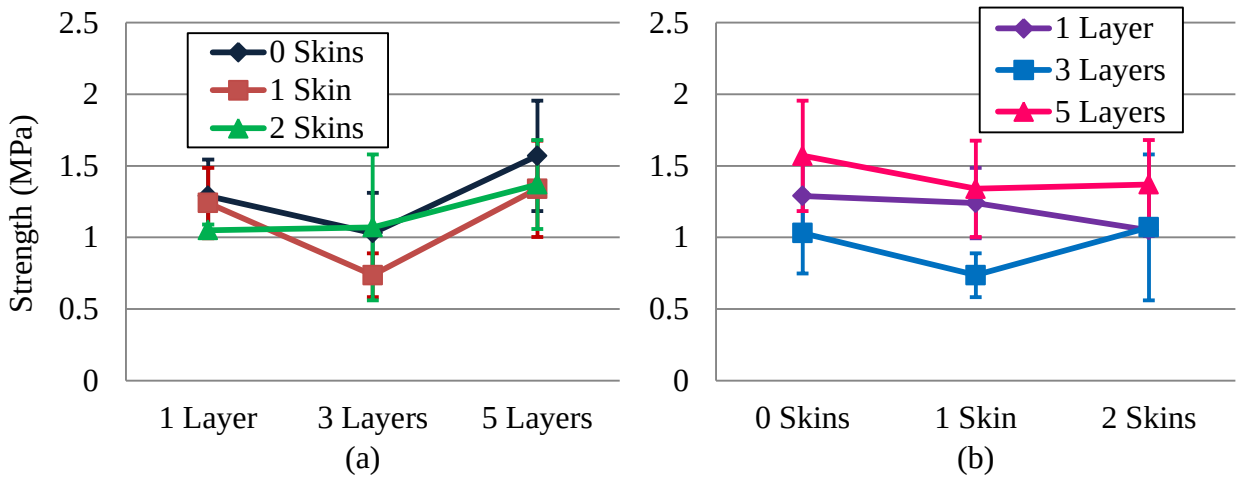

Figure 16: Plots of (a) ultimate flatwise tensile strength vs. number of layers for the CLSes with 0, 1, and 2 Skins and (b) ultimate flatwise tensile strength vs. number of skins for the CLSes with 1, 3, and 5 Layers.

In ASTM C364 [12], compressive properties of the CLSes are determined by applying an increasing compressive force in a direction parallel with the skins of a sandwich construction. According to the standard the calculation of the ultimate edgewise compressive strength involves twice the skin thickness, since sandwich constructions have two skins. However, since not all of the test specimens have two skins, the test was modified to allow the calculation of an "effective" ultimate edgewise compressive strength by modifying the calculation such that the entire thickness was used in lieu of twice the thickness of the skin. Figure 17 displays a schematic of the test configuration, and Table 7 displays the values resulting from the ASTM C364 tests. Plots of these values follow in Figure 18, which displays the calculated "effective" ultimate edgewise compressive strength with respect to the number of layers and the number of skins. Data points are mean values of results from five runs, and error bars are one standard deviation.

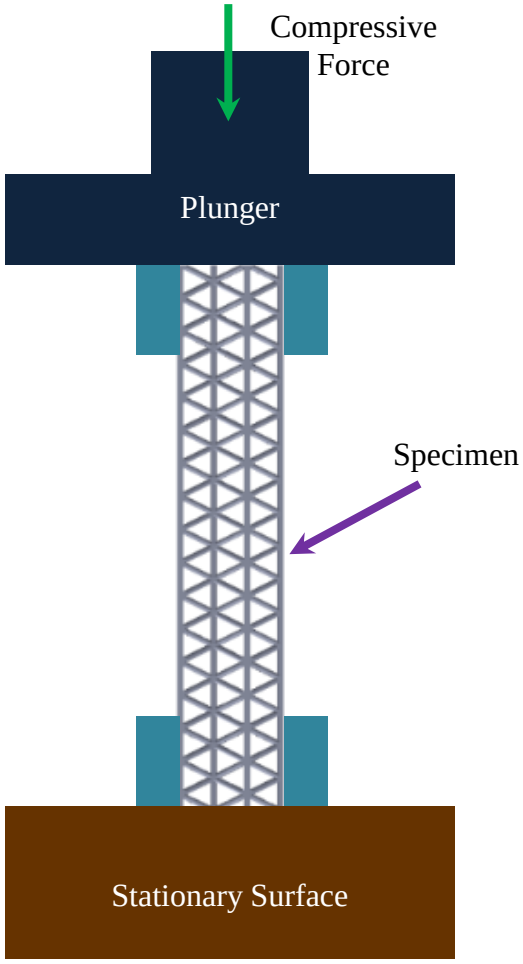

Figure 17: Schematic ASTM C364 test arrangement.

Table 7: Properties determined from the ASTM C364 testing procedures.

Label	"Effective" Ultimate Edgewise Compressive Strength MPa
1L0S	2.33
1L1S	6.99
1L2S	9.40
3L0S	1.20
3L1S	1.41
3L2S	2.52
5L0S	1.58
5L1S	2.06
5L2S	4.03

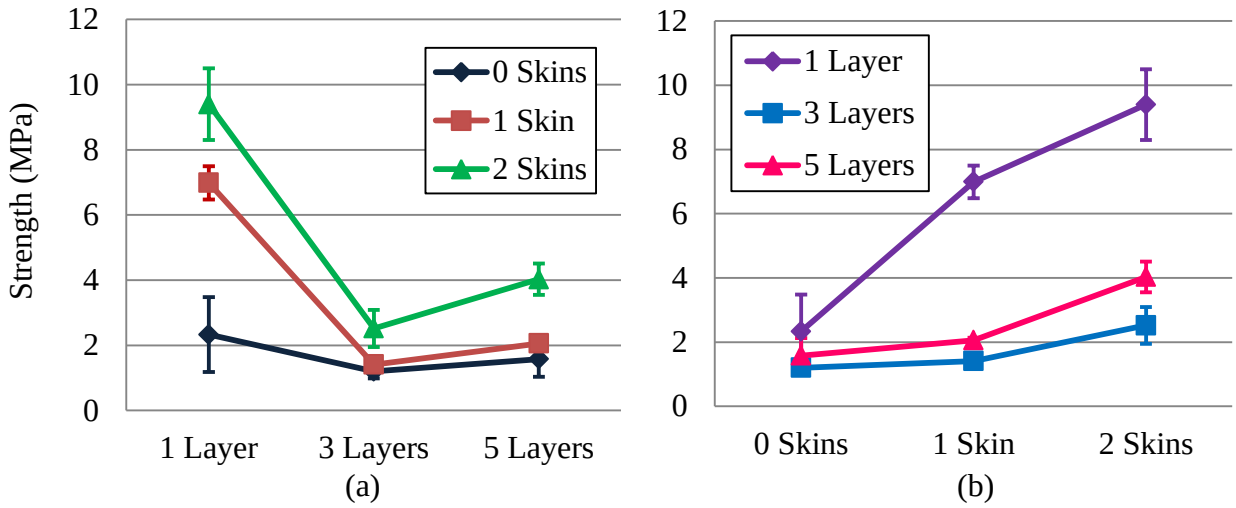

Figure 18: "Effective" ultimate edgewise compressive strength vs. (a) the number of layers for the CLSes with 0, 1, and 2 skins and (b) the number of skins for the CLSes with 1, 3, and 5 layers.

The next test performed on the bulk material properties for CLS was ASTM C273 [13]. In these tests, the shear strength parallel to the plane of a sandwich construction and the shear modulus associated with strains in a plane normal to the facings are determined. The specimen is subjected to increasing shear force parallel to the plane of its faces. Loading plates are bonded to the specimen and undergo opposing tensile or compressive (tensile for these tests) displacements resulting in a shear force on the sandwich core. Figure 19 shows an illustration of the test schematic. The data recorded during the test is used to determine the ultimate shear strength.

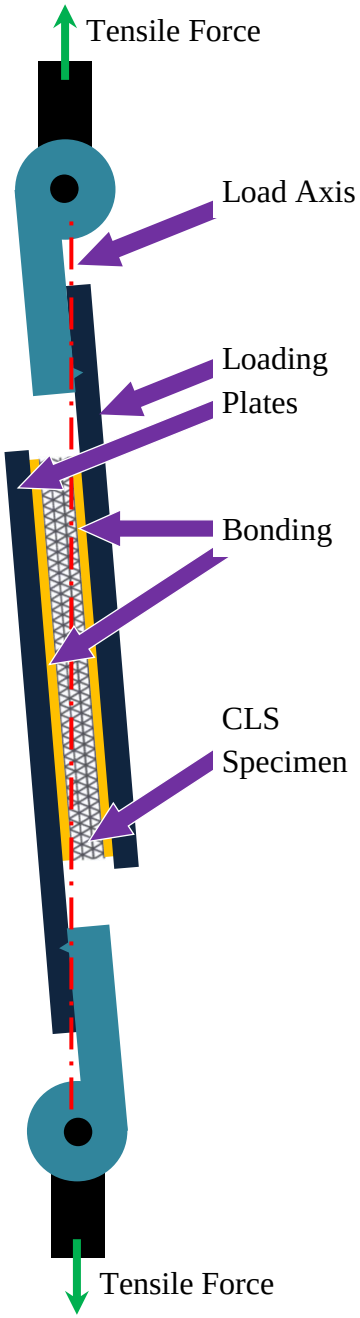

Figure 19: Schematic of ASTM C273 test setup.

Table 8 displays the values resulting from the ASTM C273 tests and plots of these values follow. Figure 20 displays plots of ultimate shear strength with respect to the number of layers and the number of skins. Each data point is the mean value of results from five tests, and the error bars represent one standard deviation.

Table 8: Property Values from the ASTM C273 Testing Procedures.

Label	Ultimate Shear Strength MPa
1L0S	17.77
1L1S	15.64
1L2S	21.24
3L0S	3.68
3L1S	6.87
3L2S	6.23
5L0S	1.80
5L1S	2.47
5L2S	2.45

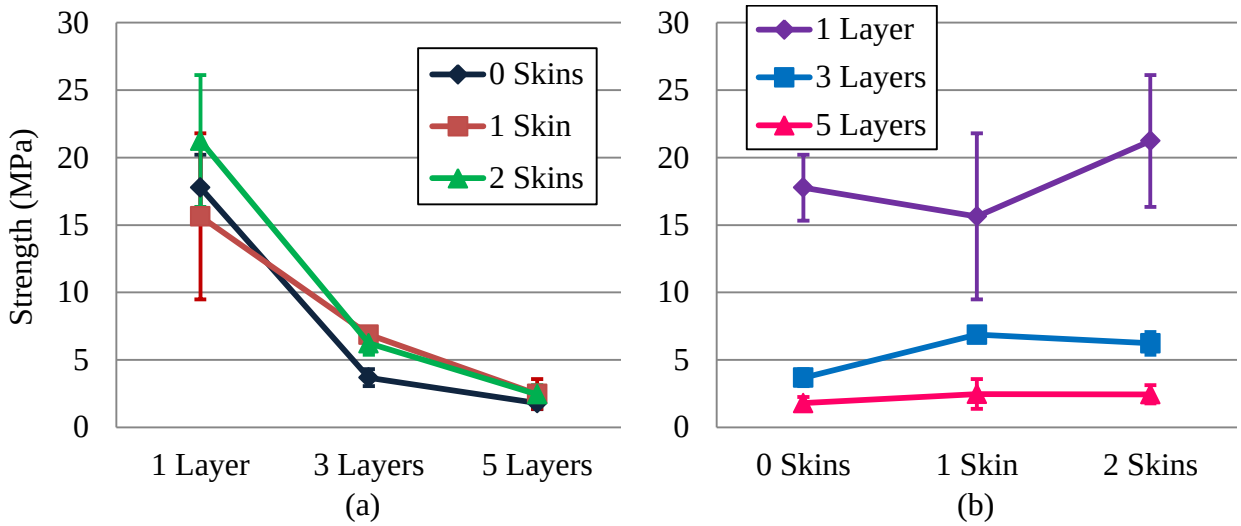

Figure 20: Ultimate shear strength vs. (a) the number of layers for the CLSes with 0, 1, and 2 skins and (b) the number of skins for the CLSes with 1, 3, and 5 layers.

During the next tests, ASTM C393 [14], three-point bending was applied to each CLS specimen to create a bending moment normal to the plane of the core, as depicted in Figure 21. The core shear ultimate strength values were then determined. Table 9 shows the values resulting from the ASTM C393 tests and plots of core shear ultimate strength with respect to the number of layers and core shear ultimate strength with respect to the number of skins follow in Figure 22. The error bars represent one standard deviation.

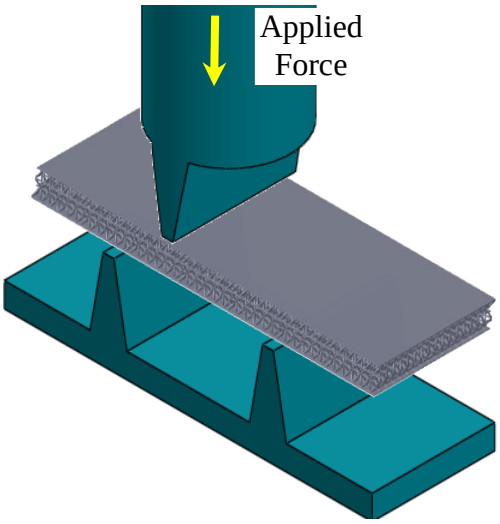

Figure 21: Schematic of ASTM C393 test setup.

Table 9: Values obtained from the ASTM C393 testing procedures.

Label	Core Shear Ultimate Strength MPa
1L0S	4.26
1L1S	6.59
1L2S	17.50
3L0S	1.83
3L1S	2.91
3L2S	5.70
5L0S	1.59
5L1S	2.25
5L2S	2.98

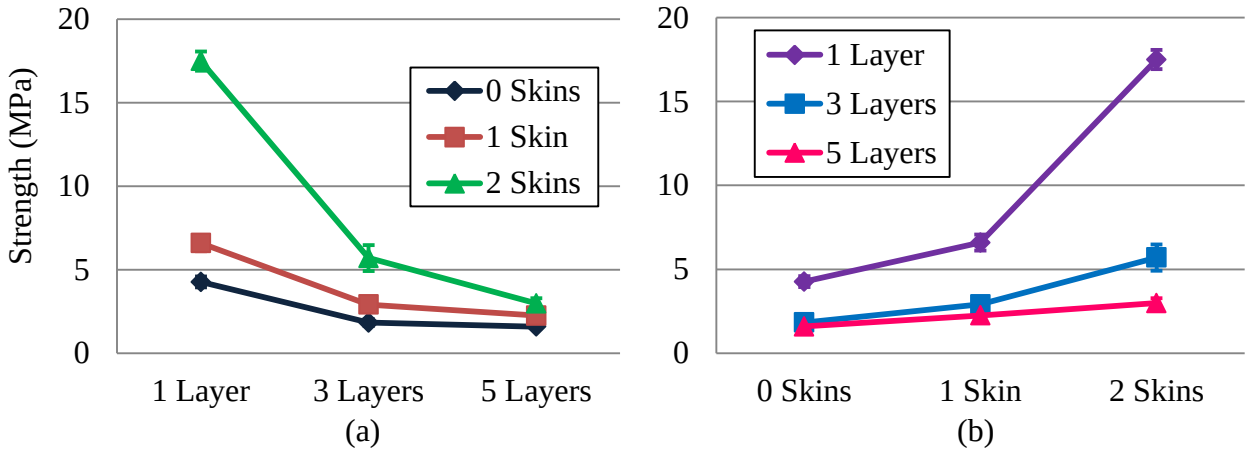

Figure 22: Core shear ultimate strength vs. (a) the number of layers for the CLSes with 0, 1, and 2 Skins and (b) the number of skins for the CLSes with 1, 3, and 5 Layers.

The next set of tests performed on the CLSes was ASTM C363 [15]. This standard is followed to determine the tensile strength of the node bond of a honeycomb core material, which determines whether the nodes of the honeycomb cores will remain intact during cutting, machining, and forming operations. A uniaxial tensile force parallel to the plane of the honeycomb is applied through pins that are placed through cell rows at the top and bottom of the specimen. Figure 23 presents a schematic of the testing arrangement with an example of a honeycomb structure loaded into the fixture.

Obstacles had to be navigated to allow determination of the tensile strength of the node bonds of the CLSes. First, performing the procedures outlined in ASTM C363 on the CLSes was not possible for two reasons: 1) the standard is designed for structures with no skins, and the nature of our investigation requires that some specimens have one or two skins; and 2) the geometry of the trusses in the core of the CLSes prevented the insertion of pins. Therefore, a modified version of ASTM D638 was employed. As previously described, tensile properties are determined in this test by subjecting specimens to an increasing uniaxial tension.

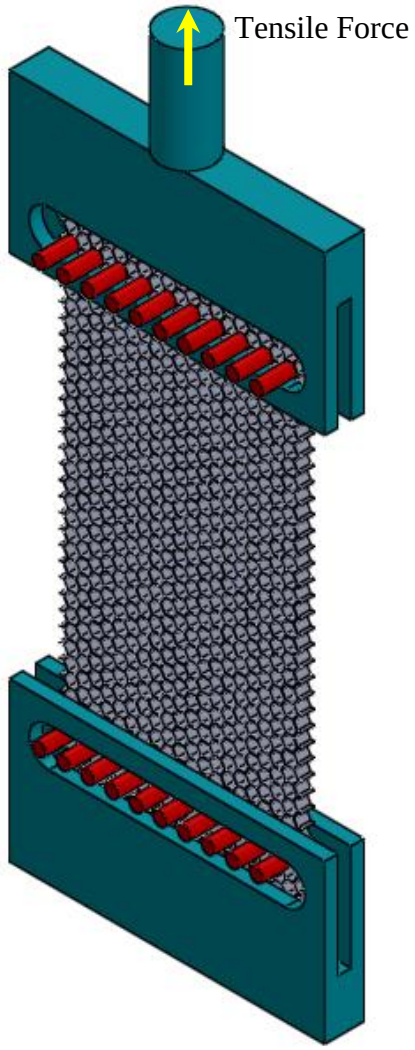

Figure 23: ASTM 363 Testing Arrangement.

However instead of testing tensile bars, the specimens were sheets dimensioned in accordance with ASTM C363. They were just clamped into the tensile tester instead of being held by pins inserted through the lattice. Additionally, the nature of the node tension test requires that there be an actual node within the core of the sample. The single-layered specimens did not satisfy this requirement, so samples with two layers were used instead. Consequently, the types of CLSes that were tested for node tensile strength differed slightly from the rest of the CLSes tested previously. Table 10 lists the CLS specimen types.

Table 10: Types of CLS specimens built for the modified ASTM D638 tests.

Label	Description
2L0S	two layers and no skins
2L1S	two layers and one skin
2L2S	two layers and two skins
3L0S	three layers and no skins
5L0S	five layers and no skins

Table 11 displays the values resulting from the modified ASTM D638 tests and plots of these data follow. Figure 24 displays plots of ultimate tensile node strength with respect to the number of layers and the number of skins. Each data point is the mean value of results from five tests, and the error bars represent one standard deviation.

Table 11: Property values obtained from the modified ASTM D638 tests.

Label	Ultimate Tensile Node Strength MPa
2L0S	1.75
2L1S	7.19
2L2S	7.89
3L0S	1.58
5L0S	1.40

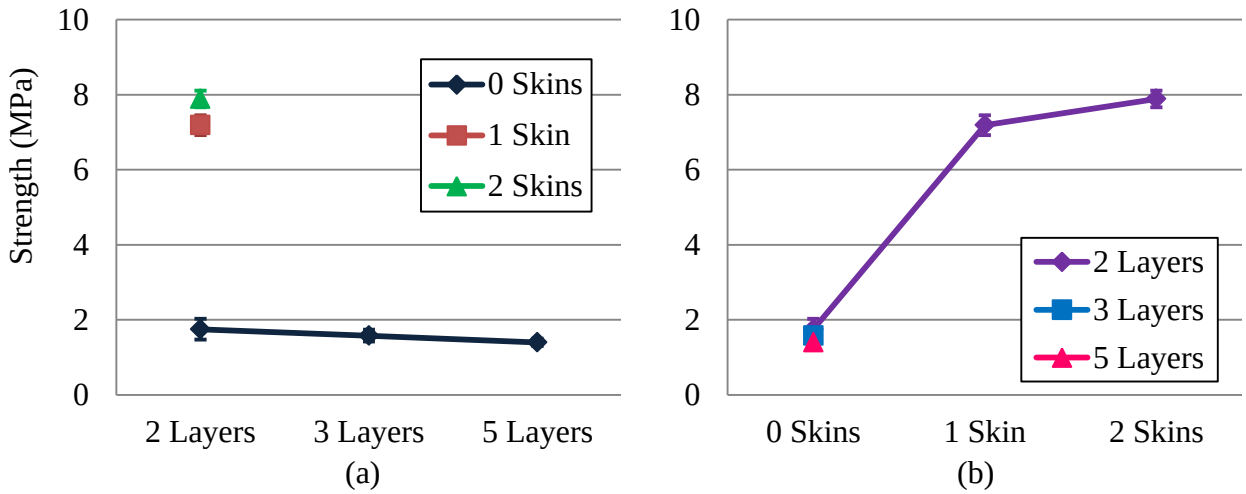

Figure 24: Plots of ultimate tensile node strength vs. (a) the number of layers the CLSes with 0, 1, and 2 Skins and (b) the number of skins for the CLSes with 2, 3, and 5 layers.

Discussion and Next Steps

A substantial amount of data has been presented in this paper. Some plots display trends that are somewhat predictable. For instance, in Figure 7(a), higher tensile strengths are expected from specimens with larger cross-sectional areas. Some plots display unexplainable phenomena, such as the plots in Figure 9(b). The cause for the drops in the compressive strength of the 2 mm struts from the values obtained during the 1 mm strut tests is unknown. Finally, some of the plots display no clear trends.

Future work will involve two areas. First, correlations between single strut properties and lattice structures need to be developed. Upon doing so, the resulting relationships could be incorporated into the simulation software used during the iterative process used in creating a CLS. Much data was captured by the outside testing facility, and a more comprehensive study of the results will provide a broader understanding of causes and effects, which aid in finessing the behavior predictions made by simulation software.

Next, regarding the bulk properties of the CLSes, there needs to be a comparison made to the bulk properties of representative samples of solid, non-latticed material. This would help fill the gap between having the capability to design CLSes and having knowledge of how to best implement them into both existing designs and those yet to be imagined. To do this, an experimental plan must be devised to identify those representative samples, and their properties need to be determined.

Conclusions

To conclude, the work described here has presented the results of numerous ASTM tests performed on single struts that together make a “peacock” structure as well as tests performed on bulk CLS structures, both fabricated via SLS. Further studies will deliver more insight on behavior trends. Another very important observation brought forth by this project is the need for

standards pertaining to lattice structures fabricated through additive manufacturing. It is evident that the applicability of already existing ASTM standards varies case-by-case. As the use of CLS technology increases, rigorous methods of testing representative geometries need to be in place.

Acknowledgements

The research presented here was funded through contract number FA8650-10-C-5705 by the United States Air Force Research Laboratory with funding provided by the Defense-wide Manufacturing Science and Technology Program through the Office of the Secretary of Defense, Manufacturing and Industrial Base Policy.

References

[1] L. J. Gibson and M. F. Ashby, *Cellular Solids: Structure and Properties*, 1997, Cambridge University Press, Cambridge, UK.

[2] M. F. Ashby, et al., *Metal Foams: A Design Guide*, 2000, Butterworth-Heinemann, Woburn, MA.

[3] S. Engelbrecht, et al., *Cellular Structures for Optimal Performance*, Solid Freeform Fabrication Symposium Proceedings, 2009, Austin, TX.

[4] J. Nguyen, et al., *Conformal Lattice Structure Design and Fabrication*, Solid Freeform Fabrication Symposium Proceedings, 2012, Austin, TX.

[5] J. Nguyen, S.-I. Park and D. W. Rosen, *Cellular structure design for lightweight components*, 5th International Conference on Advanced Research and Rapid Prototyping Proceedings, 2011, Leiria, Portugal.

[6] O. Cansizoglu, et al., *Properties of Ti-6Al-4V non-stochastic lattice structures fabricated via electron beam melting*, Materials Science and Engineering: A, 2008, **492**(1-2), pp. 468-474.

[7] A. L. Cooke, *Selective Laser Sintering (SLS) of Next Gen Unmanned Air Vehicles (UAVs)*, RAPID, 2013, Pittsburgh, PA.

[8] ASTM, *D638 - 08 Standard Test Method for Tensile Properties of Plastics*, 2008.

[9] ASTM, *D695 - 10 Standard Test Method for Compressive Properties of Rigid Plastics*, 2010.

[10] ASTM, *D790 - 10 Standard Test Methods for Flexural Properties of Unreinforced and Reinforced Plastics and Electrical Insulating Materials*, 2010.

[11] ASTM, *C297 / C297M - 04(2010) Standard Test Method for Flatwise Tensile Strength of Sandwich Constructions*, 2010.

[12] ASTM, *C364 / C364M - 07(2012) Standard Test Method for Edgewise Compressive Strength of Sandwich Constructions*, 2012.

[13] ASTM, *C273 / C273M - 11 Standard Test Method for Shear Properties of Sandwich Core Materials*, 2011.

[14] ASTM, *C393 / C393M - 11e1 Standard Test Metod for Core Shear Properties of Sandwich Constructions by Beam Flexure*, 2011.

[15] ASTM, *C363 / C363M - 09 Standard Test Method for Node Tensile Strength of Honeycomb Core Materials*, 2009.